Sun *et al. Skeletal Muscle* (2025) 15:2
https://doi.org/10.1186/s13395-024-00371-1

Skeletal Muscle

RESEARCH Open Access

Aminoguanidine hemisulfate improves mitochondrial autophagy, oxidative stress, and muscle force in Duchenne muscular dystrophy via the AKT/FOXO1 pathway in mdx mice

Shiyue Sun[1,2,3†], Tongtong Yu[2†], Joo Young Huh[4,5], Yujie Cai[2], Somy Yoon[1*] and Hafiz Muhammad Ahmad Javaid[2*]

Abstract

Background Duchenne muscular dystrophy (DMD) is a prevalent, fatal degenerative muscle disease with no effective treatments. *Mdx* mouse model of DMD exhibits impaired muscle performance, oxidative stress, and dysfunctional autophagy. Although antioxidant treatments may improve the *mdx* phenotype, the precise molecular mechanisms remain unclear. This study investigates the effects of aminoguanidine hemisulfate (AGH), an inhibitor of reactive oxygen species (ROS), on mitochondrial autophagy, oxidative stress, and muscle force in *mdx* mice.

Methods Male wild-type (WT) and *mdx* mice were divided into three groups: WT, *mdx*, and AGH-treated *mdx* mice (40 mg/kg intraperitoneally for two weeks) at 6 weeks of age. Gene expression, western blotting, H&E staining, immunofluorescence, ROS assays, TUNEL apoptosis, glutathione activity, and muscle force measurements were performed. Statistical comparisons used one-way ANOVA.

Results AGH treatment significantly reduced the protein levels of LC3, and p62 in *mdx* mice, indicating improved autophagy activity and the ability to clear damaged mitochondria. AGH restored the expression of mitophagy-related genes *Pink1* and *Parkin* and increased *Mfn1*, rebalancing mitochondrial dynamics. It also increased *Pgc1a* and *mtTFA* levels, promoting mitochondrial biogenesis. ROS levels were reduced, with higher Prdx3 and MnSOD expression, improving mitochondrial antioxidant defenses. AGH normalized the GSSG/GSH ratio and decreased glutathione reductase and peroxidase activities, further improving redox homeostasis. Additionally, AGH reduced apoptosis, shown by fewer TUNEL-positive cells and lower caspase-3 expression. Histological analysis revealed decreased muscle damage and fewer embryonic and neonatal myosin-expressing fibers. AGH altered fiber composition, decreasing

†Shiyue Sun and Tongtong Yu contributed equally as first author.

*Correspondence:
Somy Yoon
somyyoon@jnu.ac.kr
Hafiz Muhammad Ahmad Javaid
hafizjavaid@wmu.edu.cn

Full list of author information is available at the end of the article

© The Author(s) 2024. **Open Access** This article is licensed under a Creative Commons Attribution-NonCommercial-NoDerivatives 4.0 International License, which permits any non-commercial use, sharing, distribution and reproduction in any medium or format, as long as you give appropriate credit to the original author(s) and the source, provide a link to the Creative Commons licence, and indicate if you modified the licensed material. You do not have permission under this licence to share adapted material derived from this article or parts of it. The images or other third party material in this article are included in the article's Creative Commons licence, unless indicated otherwise in a credit line to the material. If material is not included in the article's Creative Commons licence and your intended use is not permitted by statutory regulation or exceeds the permitted use, you will need to obtain permission directly from the copyright holder. To view a copy of this licence, visit http://creativecommons.org/licenses/by-nc-nd/4.0/.

MyH7 while increasing *MyH4* and *MyH2*. Muscle force improved significantly, with greater twitch and tetanic forces. Mechanistically, AGH modulated the AKT/FOXO1 pathway, decreasing myogenin and Foxo1 while increasing MyoD.

Conclusions AGH treatment restored mitochondrial autophagy, reduced oxidative stress, apoptosis, and altered muscle fiber composition via the *AKT/FOXO1* pathway, collectively improving muscle force in *mdx* mice. We propose AGH as a potential therapeutic strategy for DMD and related muscle disorders.

Keywords *Mdx*, ROS, Autophagy, Mitochondria, Aminoguanidine, Apoptosis, DMD

Background

Duchenne muscular dystrophy (DMD) is a prevalent X-linked fatal disorder characterized by the progressive weakening and degeneration of skeletal muscles [1, 2]. This condition arises from mutations in the dystrophin gene, leading to dystrophin deficiency [2, 3]. Despite significant advances in gene- and cell-based therapies, a definitive cure for DMD remains elusive, highlighting the critical need for innovative therapeutic approaches to address this unmet clinical need.

Oxidative stress is a pivotal factor in the pathophysiology of DMD that contributes significantly to muscle degeneration [4–6]. Mitochondria play essential roles in energy production, reactive oxygen species (ROS) generation, signal transduction, and apoptosis [7]. Therefore, maintaining mitochondrial homeostasis requires a delicate balance between biosynthesis and degradation processes [8]. Transcriptional regulators such as peroxisome proliferator-activated receptor gamma coactivator-1 alpha (Pgc1α) are integral to mitochondrial biogenesis [9]. Conversely, the elimination of dysfunctional or surplus mitochondria depends on mitophagy, a specialized form of autophagy that targets impaired mitochondria [10]. The proteins PTEN-induced putative kinase (Pink1) and Parkin are critical in identifying and tagging damaged mitochondria for autophagic clearance [11].

Mitigating oxidative stress is crucial for maintaining skeletal muscle homeostasis. In the context of DMD, antioxidants have shown promise as therapeutic agents [6, 12, 13]. Aminoguanidine hemisulfate (AGH) is an inhibitor of both nitric oxide synthase and ROS. In vitro studies have demonstrated that AGH effectively reduces ROS production induced by areca nut extract [14]. Additionally, AGH has been used to treat systemic granulomatous diseases such as paracoccidioidomycosis [15]. However, research remains limited on the effectiveness of AGH in ameliorating skeletal muscle damage in the *mdx* mouse model of DMD, which closely mimics the characteristics of human DMD.

In the context of skeletal muscle homeostasis, FOXO transcription factors, particularly FOXO1, play a central role in the regulation of genes involved in antioxidant defense, cell-cycle arrest, and apoptosis [16]. FoxO1 mRNA is widely expressed across various skeletal muscles [17], and the AKT/FOXO1 signaling pathway is involved in skeletal muscle differentiation [18]. Moreover, Foxo1 has a significant role in muscle regeneration, injury response, and modulating fiber type composition [19, 20]. Given the importance of these functions in maintaining muscle integrity, the AKT/FOXO1 pathway may be a key mediator of muscle repair processes.

Given the critical roles of oxidative stress and mitochondrial dysregulation in DMD progression, we hypothesize that AGH supplementation represents a promising therapeutic strategy for mitigating muscle degeneration. Through experiments on the *mdx* mouse model, we propose that AGH enhances mitochondrial autophagy, reduces oxidative stress, and modulates the key signaling pathways involved in muscle homeostasis. Specifically, we suggest that AGH improves skeletal muscle performance in young *mdx* mice by regulating mitochondrial autophagy and influencing pathological features through the *AKT*/*FOXO1* signaling pathway. This study is novel in its exploration of the effects of AGH on mitochondrial dynamics and muscle force in DMD, an area that has not been thoroughly examined. By investigating these mechanisms, our research provides new insights that can inform the development of targeted therapeutic strategies for DMD, thereby addressing the urgent need for more effective DMD treatments.

Materials and methods

Experimental animals and AGH treatment

6 weeks old male wild-type (WT; C57BL/6; $n = 10$) and *mdx* (C57BL/6JGpt-Dmdem10Cd580/Gpt; $n = 10$) mice were purchased from GemPharmatech Company (Nanjing, China) and housed in the Laboratory Animal Center of Wenzhou Medical University. Mice were conventionally housed in temperature- and humidity-controlled rooms with a 12-h light:12-h dark cycle and food and water available ad libitum. AGH was purchased from MCE (HY-W020772, MedChemExpress, China). Mice were assigned to three different experimental groups: WT, *mdx*, and *mdx* + AGH. Mice in the *mdx* + AGH group were treated with 40 mg/kg AGH by intraperitoneal injection daily for 2 weeks [21], while mice in WT and *mdx* groups were injected with vehicle ddH2O. At 8 weeks of age, all mice were sacrificed and the tibialis anterior muscle (TA) was harvested for subsequent experiments. All experiments were conducted in accordance

with the Guide for the Care and Use of Laboratory Animals. This study was approved by the Animal Studies Ethics Committee of Wenzhou Medical University.

Gene expression analysis

Total RNA was extracted from tissue using TRIzol reagent (TaKaRa, Shiga, Japan). Complementary DNA was synthesized using the RevertAid First Strand cDNA Synthesis Kit (K1622, Thermo Scientific, Vilnius, Lithuania). mRNA levels were measured by real-time PCR with a Rotor-Gene Q (QIAGEN; Hilden, Germany) with a 10 μl reaction volume consisting of cDNA transcripts in TB Green Premix Ex Taq II (RR820B, TaKaRa, Shiga, Japan). Gene expression levels were normalized against 36B4. The primers used in this study are listed in Supplementary Table 1.

Western blot

Briefly, TA muscle samples were lysed on ice in RIPA buffer (Thermo Scientific, Rockford, IL, USA). Protein concentrations were determined using a BCA kit (Thermo Scientific), and equal amounts of protein samples were separated by SDS–PAGE and transferred onto PVDF membranes. The membranes were blocked with 5% skim milk for 1 h at room temperature then incubated with primary antibodies overnight at 4 °C. Following overnight incubation, the membranes were washed with Tris-buffered saline containing Tween-20 and subsequently incubated with secondary antibodies for 1 h at room temperature. After washing, protein bands on the blots were visualized using a Clinx-6100 chemiluminescence imaging system (Clinx Science Instruments, Shanghai, China).

Primary antibodies against LC3 (14600-1-AP, 1:1,000), p62 (18420-1-AP, 1:1,000), Pink1 (23274-1-AP, 1:1,000), Prdx3 (10664-1-AP, 1:1,000), Foxo1 (18592-1-AP, 1:1,000), MyH7 (22280-1-AP, 1:1,000), myosin-embryonic (22287-1-AP, 1:1,000), MnSOD (66474-1-Ig, 1:1,000), goat anti-rabbit IgG-HRP (SA00001-2, 1:5,000), and goat anti-mouse IgG-HRP (SA00001-1, 1:5,000) were purchased from Proteintech (Wuhan, China). Antibodies against phospho-AKT (#9271, 1:2,000), total AKT (#9272, 1:2,000), and β-tubulin (#2146, 1:2,000) were obtained from Cell Signaling Technology (Danvers, MA, USA). Myosin-neonatal (sc-53097, 1:1,000), MyoD (sc-32758, 1:1,000), and myogenin (sc-12732, 1:1,000) were purchased from Santa Cruz Biotechnology, Inc. (Dallas, TX, USA), whereas phospho-Foxo1 (12198, 1:1,000) and myosin-embryonic (bs-10905R, 1:200) were sourced from SAB Biotherapeutics, Inc. (Sioux Falls, SD, USA) and Bioss (Beijing, China), respectively.

Hematoxylin and eosin and immunofluorescence staining

TA muscles were harvested and immediately fixed in paraformaldehyde (Beyotime, Shanghai, China). After fixation, the tissues were embedded in paraffin according to a standard protocol and sectioned at a thickness of 5 μm. For a general assessment of tissue morphology, the sections were stained with hematoxylin and eosin. For specific protein visualization, deparaffinized tissues were unmasked using an antigen unmasking solution (Vector Laboratories, Burlingame, CA, USA) in a microwave oven. After being blocked in 5% goat serum (Beyotime) for 30 min, the sections were incubated with primary antibodies overnight at 4 °C. These antibodies of interest were same as those used in western blotting. The following day, sections were washed with PBS and then incubated with the appropriate secondary antibody for 1 h at room temperature The secondary antibodies used were Alexa Fluor 594-conjugated goat anti-rabbit IgG (A32740, 1:1000) and Alexa Fluor 594-conjugated goat anti-mouse IgG (A32742, 1:1000), purchased from Thermo Scientific. DAPI was used for nuclear staining, and sections were imaged using a Leica DM6000B microscope (Leica Microsystems) under consistent conditions, including blocking, antibody incubation, washing, exposure time, and imaging parameters. Fluorescence intensity was quantified using ImageJ software (NIH, Bethesda, MD, USA). To ensure specificity, only muscle sections exhibiting clear injury or damage, as identified by H&E staining, were analyzed. These damaged sections were randomly selected from muscle cross-sections to minimize bias.

To account for potential variability in fluorescence intensity, background fluorescence was corrected by subtracting intensity values from negative control images. The intensity measurements were normalized across all images to control for differences in imaging parameters. All analyses were performed by an investigator blinded to group allocation.

ROS assays

ROS levels in the TA muscle were evaluated using a 2′,7′-Dichlorodihydrofluorescein diacetate (DCFH-DA) kit (S0033S, Beyotime) anda dihydroethidium (DHE) fluorescent probe kit (S0063, Beyotime). Briefly, fresh tissue lysates were prepared and incubated with either 10 μM DCFH-DA for 20 min in the dark at room temperature or 10 μM DHE at 25 °C in the dark for 1 h, following the manufacturer's instructions. ROS production was quantified using a Varioskan LUX microplate reader (Thermo Scientific). Mitochondrial ROS was measured by mitochondrial superoxide indicator (MitoSOX, HY-D1055, MCE, China). Briefly, fresh TA muscle samples were embedded in optimum cutting temperature (OCT) compound and sectioned at a thickness of 5 μm to prepare

frozen sections. The sections were then incubated with MitoSOX solution (5 μM) at 37 °C for 30 min following the manufacturer's instructions. All stained sections were imaged by a Leica DM6000B microscope (Leica Microsystems).

TUNEL apoptosis assay

For the apoptosis assay, sections were processed using a One Step TUNEL apoptosis assay kit (C1089, Beyotime) according to the manufacturer's instructions. TUNEL-positive cells were observed using a Leica DM6000B microscope.

Glutathione and MnSOD activity assays

Total glutathione (GSH) and oxidized glutathione (GSSG) concentrations were measured using GSH and GSSG assay kits (S0053, Beyotime) according to the manufacturer's instructions. GSH reductase and GSH peroxidase activities were assessed using the GSH reductase assay kit with DTNB (S0055, Beyotime) and the GSH peroxidase assay kit with NADPH (S0056, Beyotime), respectively. Additionally, MnSOD activity in TA muscle was measured using the MnSOD Assay Kit (S0103, Beyotime).

Grip strength and muscle force measurements

Grip strength was measured as previously described [22, 23]. Mice were placed on a grip strength meter (YR92-YLS-13 A, M281330), ensuring they gripped the mesh with both their forelimbs and hind limbs. The mice were then pulled horizontally by the tail until they lost their grip. Each mouse underwent five trials, and the maximum force generated during each trial was recorded. The average force across the five trials was calculated for each animal. Grip strength data were normalized to body weight to account for potential variations in animal size. In situ TA force measurements were performed using the RM6240 signal acquisition system (Chengdu Instrument Factory, Chengdu, China) following a previous protocol with slight modifications [24]. Briefly, the mice were anesthetized with 1% pentobarbital after 2 weeks of AGH treatment. The TA muscle was exposed, and the distal tendon was freed from the connective tissue and attached to the mechanical force transducer with a 6–0 suture and subjected to stimulation via 0.2-s pulses at a voltage of 5 V, followed by a rest period after each pulse. Isometric measurements were conducted at the initial muscle length, which was established by applying successive single-twitch stimulations and adjusting the basal muscle tension until the maximal isometric twitch force was attained. The muscle was subsequently stimulated at various frequencies to determine the absolute maximum tetanic force. Both twitch and tetanic forces were normalized to the TA muscle mass to account for potential variations in muscle size.

Statistical analysis

The data were analyzed using Statview v5.0 (SAS Institute Inc., Cary, NC, USA). Values were presented as the means ± standard errors of the means of triplicate experiments. Shapiro-Wilk test was used to examine the normality of the data. Statistical comparisons between groups were determined by one-way analysis of variance, followed by Fisher's protected least significant difference post hoc test. Graphs were generated using GraphPad Prism 8.0 (San Diego, CA, USA). p values < 0.05 were considered to indicate statistical significance.

Results

AGH restores autophagy dysregulation and mitochondrial homeostasis in *mdx* mice.

The *mdx* mouse model, characterized by an absence of muscular dystrophin, is a well-established model for studying DMD. Our initial investigation focused on evaluating the accumulation of damaged mitochondria in the TA muscle of *mdx* mice. We observed a significant increase in the protein expression levels of LC3I, LC3II, and p62 in *mdx* mice compared to WT mice (Figure S1A–B). These elevated levels indicate impaired autophagosome degradation, resulting in the accumulation of damaged mitochondria in the muscles of *mdx* mice.

Given the observed impairment in autophagy activity, we next explored whether AGH treatment could enhance the mitophagy-mediated clearance of damaged mitochondria. After treating *mdx* mice with AGH, we noted a significant reduction in the protein levels of LC3I, LC3II, and p62 (Fig. 1A–E), indicating restoration of the autophagic activity. Notably, autophagy inhibition observed in the TA muscle was associated with a decrease in the mtDNA content, a condition that was reversed following AGH treatment (Fig. 1F). These results suggest that AGH effectively mitigates mtDNA damage induced by autophagy suppression in *mdx* muscle.

To further elucidate the mechanisms behind these changes, we assessed the expression of markers related to mitophagy, mitochondrial dynamics, and biogenesis. We found that the expression levels of the mitophagy-related genes *Pink1* and *Parkin* were reduced in untreated *mdx* mice but restored following AGH treatment (Fig. 1G). Additionally, AGH treatment reversed the decrease in *Mfn1* expression observed in *mdx* mice, whereas *Drp1* levels remained unchanged (Fig. 1H). This suggests that AGH promotes a rebalancing of mitochondrial dynamics, potentially contributing to improving mitochondrial health.

Moreover, AGH treatment in *mdx* mice significantly restored the expression levels of *Pgc1α* and *mtTFA*, which are key regulators of mitochondrial biogenesis (Fig. 1I). This restoration of biogenesis markers indicated the reactivation of mitochondrial biogenesis pathways

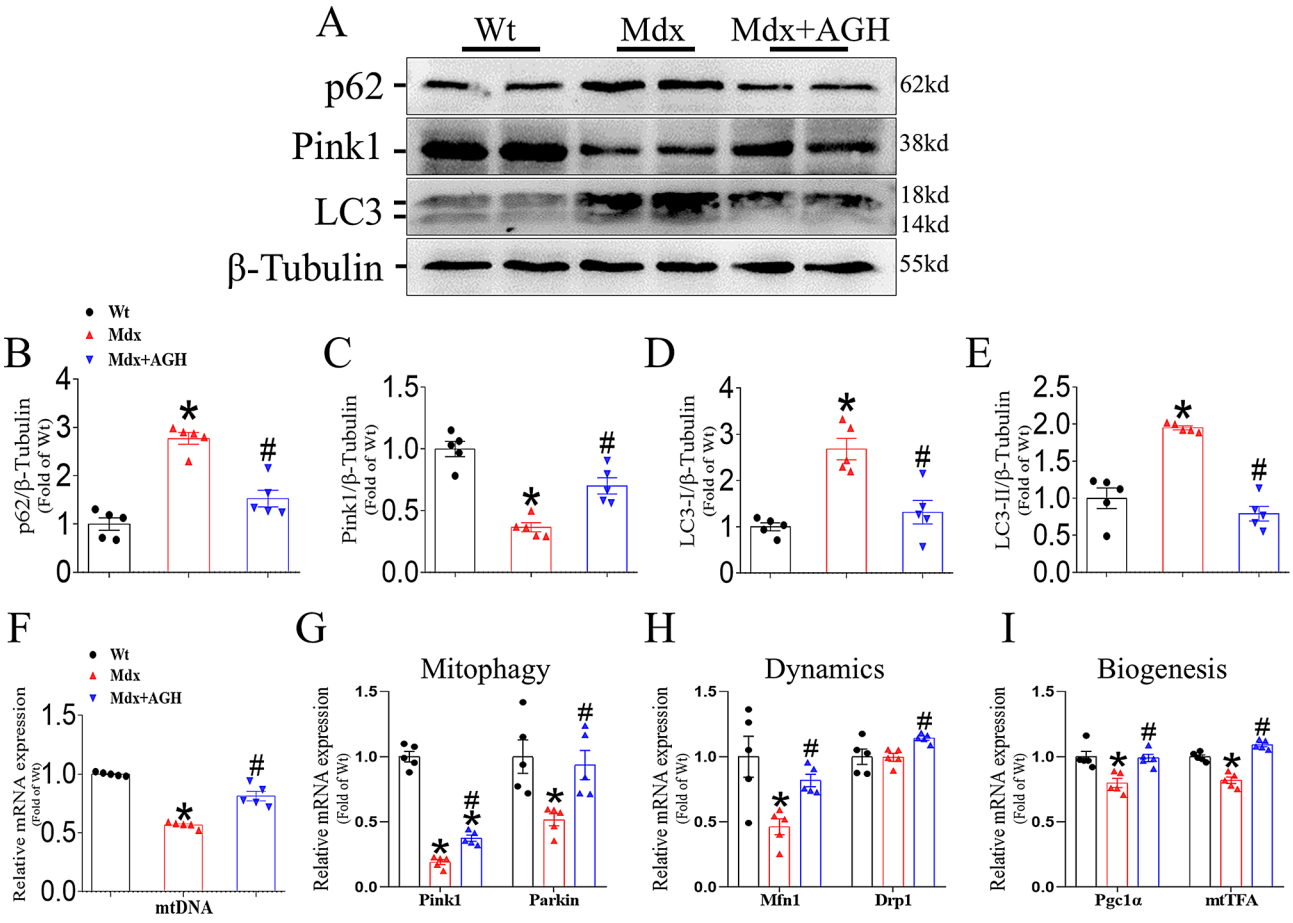


Fig. 1 Impact of AGH treatment on autophagy and mitochondrial homeostasis in the tibialis anterior (TA) muscles of *mdx* mice. TA from wild-type (WT), *mdx*, and AGH-treatment *mdx* mice were isolated at 8 weeks of age (**A**–**E**) Representative blots and quantification for LC3, p62, and Pink1. Quantitatifications were normalized to β-tubulin level. Gene expression levels of (**F**) mitochondrial DNA, (**G**) mitophagy, (**H**) mitochondrial dynamics, and (**I**) biogenesis markers were measured using real-time PCR. Values were normalized to 36B4 for each target. Values are presented as the mean ± standard error of the mean for each experiment ($n = 5$). * $p < 0.05$ compared with WT control, # $p < 0.05$ compared with *mdx*

that were downregulated in the disease state. Consistent with these findings, immunofluorescence analysis demonstrated similar trends in the expression of LC3, p62, and Pink1 proteins (Fig. 2), further confirming the impact of AGH on autophagy and mitophagy pathways. Collectively, these results suggest that AGH treatment not only rescues dysregulated autophagy but also restores mitochondrial homeostasis, thereby positively influencing mitophagy, mitochondrial dynamics, and biogenesis in *mdx* mice.

AGH decreases mitochondrial oxidative stress in *mdx* mice

Mitochondria are the primary source of ROS in eukaryotic cells, generating over 90% of these molecules in addition to ATP production [25]. DHE and DCF assays revealed that AGH treatment significantly reduced ROS levels in the TA muscle of mdx mice (Fig. 3A–C), which was further supported by MitoSOX Red staining, showing a similar reduction in mitochondrial ROS within the TA muscle (Fig. 3D–E). Furthermore, AGH treatment significantly improved mitochondrial antioxidant defense in *mdx* mice. Specifically, the protein expression of Prdx3 and MnSOD were notably decreased in *mdx* mice, which were effectively restored by AGH treatment (Fig. 3F–G). Correspondingly, gene expression analysis of *Prdx3* and *MnSOD* further confirmed these findings, showing significant improvements following AGH treatment (Fig. 3H). Moreover, AGH treatment also significantly increased MnSOD activity in *mdx* mice (Fig. 3I), and immunofluorescence staining revealed a similar trend, with AGH effectively restoring the reduced levels of Prdx3 in the TA muscle (Fig. 3J–K). These findings indicate that AGH treatment effectively attenuates ROS, mitochondrial oxidative stress and enhances mitochondrial antioxidant defenses in *mdx* mice.

AGH regulates glutathione metabolism and apoptosis

To further assess redox homeostasis, we analyzed the ratio of reduced GSH to oxidized GSSG (Fig. 4A). AGH treatment significantly attenuated the increase in total

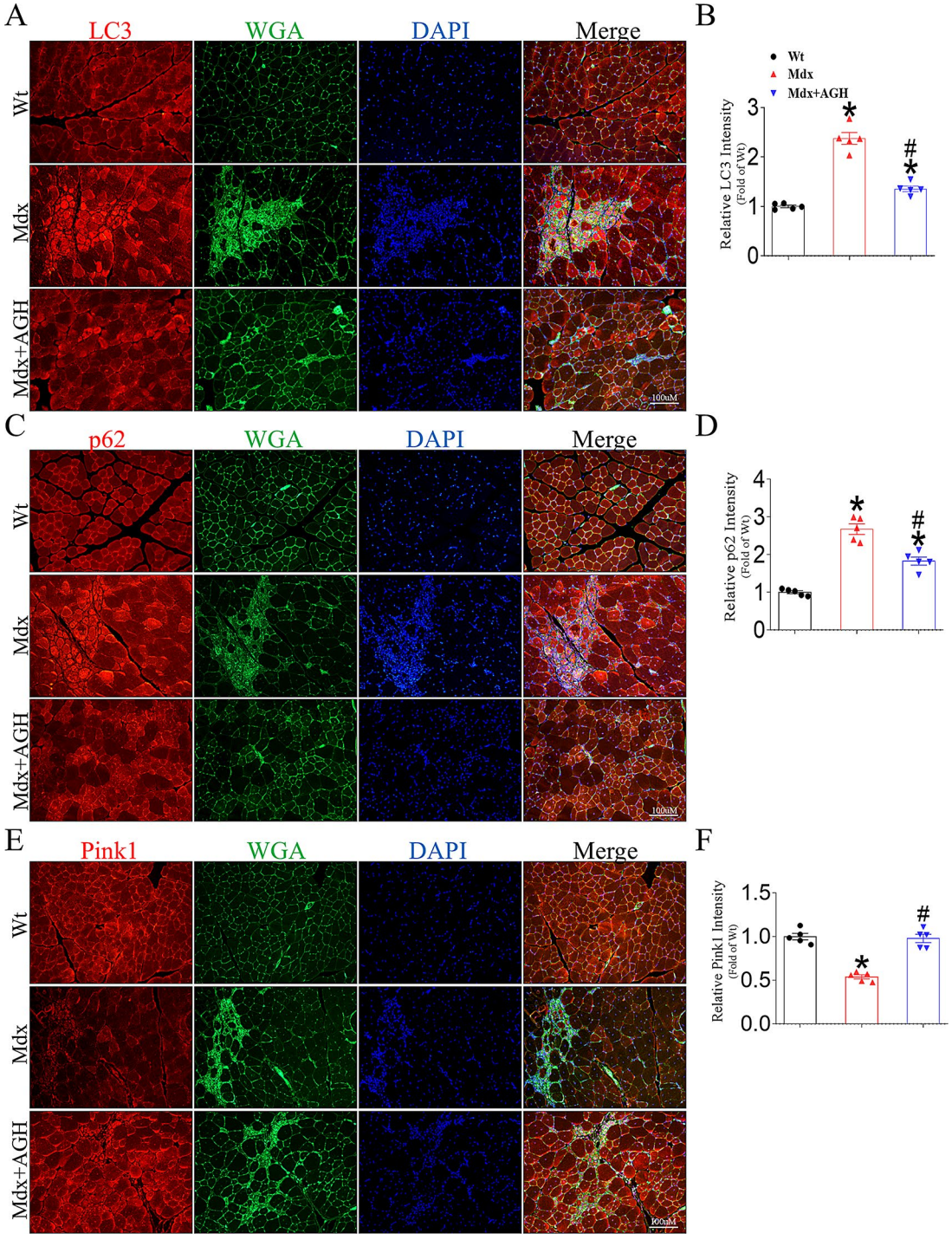


Fig. 2 AGH treatment restored autophagy in *mdx* mice. TA muscles from WT, *mdx*, and AGH-treatment *mdx* mice were isolated at 8 weeks of age. Representative immunofluorescence images and quantifications for (**A**–**B**) LC3 (arrows representing autophagosomes), (**C**–**D**) p62, (**E**–**F**) Pink1 (red), wheat germ agglutinin (WGA, green), and DAPI (blue, 20× magnification, scale bar = 100 μm). Quantification of fluorescence intensities using ImageJ software. Values are presented as the mean ± standard error of the mean for each experiment ($n = 5$). * $p < 0.05$ compared with WT control, # $p < 0.05$ compared with *mdx*

GSH and GSSG observed in *mdx* mice (Fig. 4B–C). However, the observed reduction in the GSH level of *mdx* mice was not significantly reversed following AGH treatment (Fig. 4D). AGH effectively reduced the activities of GSH reductase and GSH peroxidase (Fig. 4E–F). Moreover, the expression of the key GSH peroxidase gene *Gpx3* was significantly lower in the *mdx* group than in the WT group, but was restored following AGH treatment.

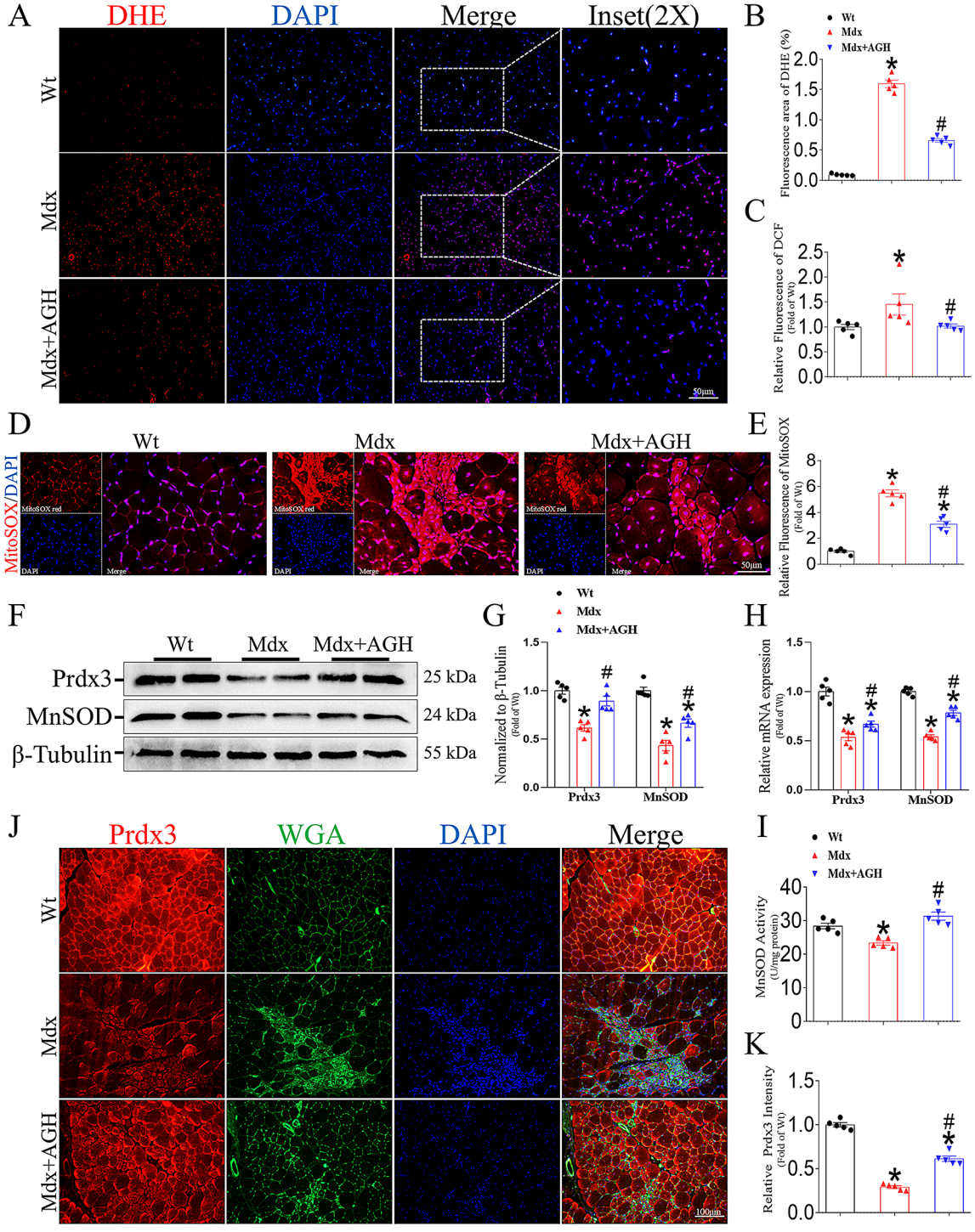


Fig. 3 AGH treatment reduced ROS. TA muscles from WT, *mdx*, and AGH-treatment *mdx* mice were isolated at 8 weeks of age. (**A**–**B**) Representative immunofluorescence images and quantification of DHE staining (red), and DAPI (blue, 20× magnification, scale bar = 50 μm). (**C**) Quantification of fluorescence intensity of DCF in fresh TA muscle by enzyme labeling. (**D**-**E**) Representative immunofluorescence images and quantification of MitoSOX staining (red), and DAPI (blue, 20× magnification, scale bar = 50 μm). (**F**–**G**) Representative blots and quantification for Prdx3 and MnSOD.Quantitatifications were normalized to β-tubulin level. Gene expression levels of (H) *Prdx3* and *MnSOD* were measured using real-time PCR. Values were normalized to 36B4 for each target. (**I**) The activity of MnSOD in TA muscle was measured per assay kit instructions. Representative immunofluorescence images and quantification for (**J**–**K**) Prdx3 (red), wheat germ agglutinin (WGA, green), and DAPI (blue, 20× magnification, scale bar = 100 μm). Values are presented as the mean ± standard error of the mean for each experiment ($n = 5$). * $p < 0.05$ compared with WT control, # $p < 0.05$ compared with *mdx*

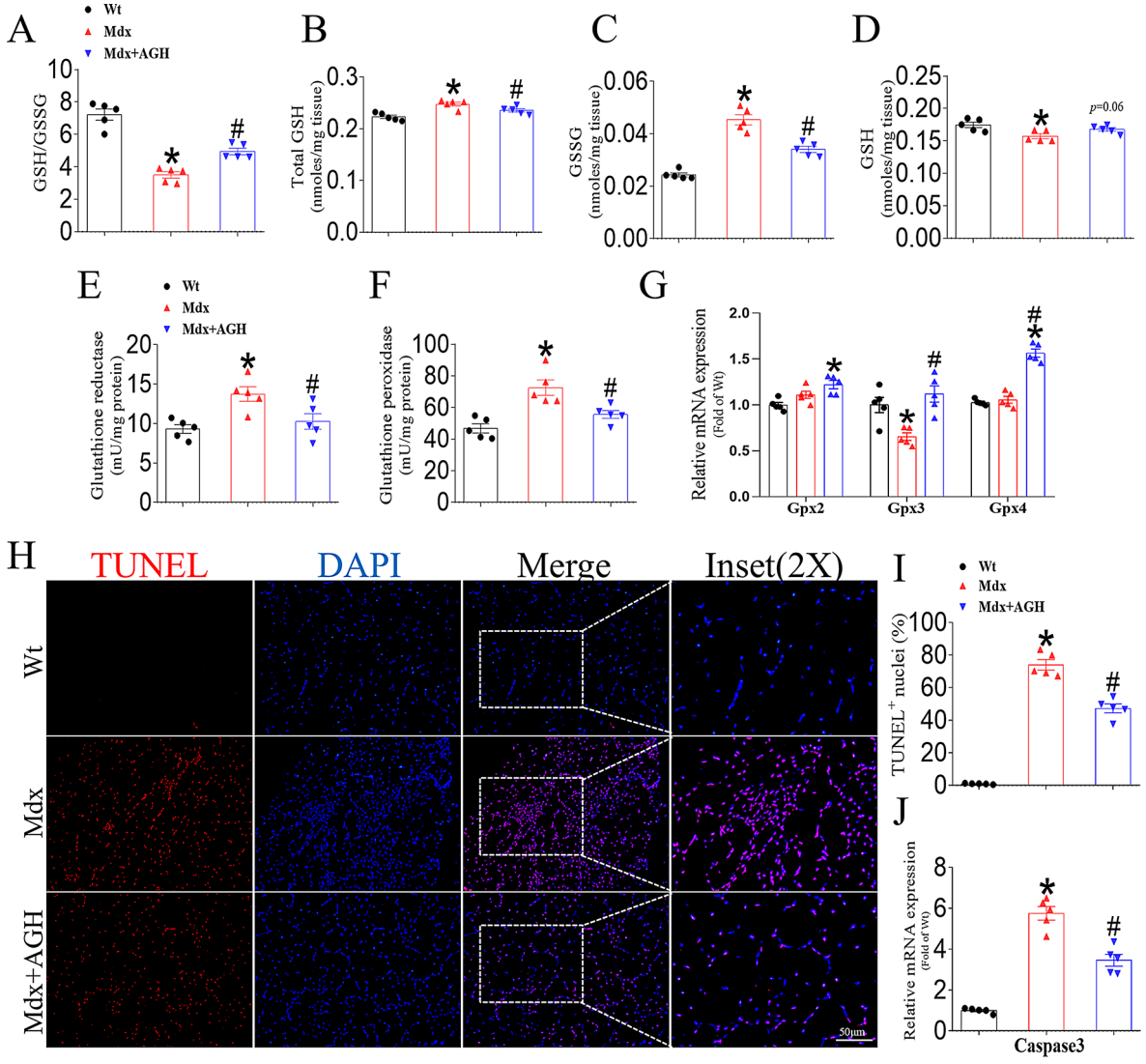


Fig. 4 AGH improved glutathione metabolism and reduced apoptosis. TA muscles from WT, *mdx*, and AGH-treatment *mdx* mice were isolated at 8 weeks of age. The ratio of (**A**) oxidized glutathione (GSSG) to glutathione (GSH) (GSSG/GSH), (**B**) the concentration of total GSH, (**C**) GSSG, and (**D**) GSH were measured per assay kit instructions. The activities of (**E**) GSH reductase and (**F**) GSH peroxidase in TA muscle were measured per assay kit instructions. Gene expression of (**G**) *Gpx2*, *Gpx3*, *Gpx4*, and (**J**) *caspase3* measured using real-time PCR. Values were normalized to 36B4 levels. (**H**–**I**) Representative images and quantification of TUNEL-positive nuclei on TA muscle (20× magnification, scale bar = 100 μm). Values are presented as the mean ± standard error of the mean for each experiment ($n = 5$). * $p < 0.05$ compared with WT control, # $p < 0.05$ compared with *mdx*

Although *Gpx2 and Gpx4* expression did not differ significantly between WT and *mdx* groups, AGH treatment notably increased the expression of both genes. (Fig. 4G). Furthermore, the number of TUNEL-positive nuclei in muscle sections and the gene expression of the apoptotic effector *caspase3* were reduced in the AGH group (Fig. 4H–J).

Taken together, these findings suggest that AGH treatment not only mitigates ROS accumulation and oxidative stress but also modulates GSH metabolism and attenuates apoptosis, thereby contributing to enhanced overall muscle health in *mdx* mice.

AGH improves muscle regeneration and fiber morphology in *mdx* mice

Next, to assess the impact of AGH treatment on muscle regeneration and fiber morphology, particularly in the context of impairment in mitochondrial autophagy we performed a histological examination of muscle tissue after AGH treatment. The results revealed a significant alleviation of the pathological features in the TA muscle of AGH-treated *mdx* mice (Fig. 5A). Furthermore, compared with *mdx*, AGH treatment decreased the proportion of centrally nucleated fibers and increased muscle fiber size (Fig. 5B–D). The proportion of skeletal muscle fibers expressing embryonic myosin and neonatal

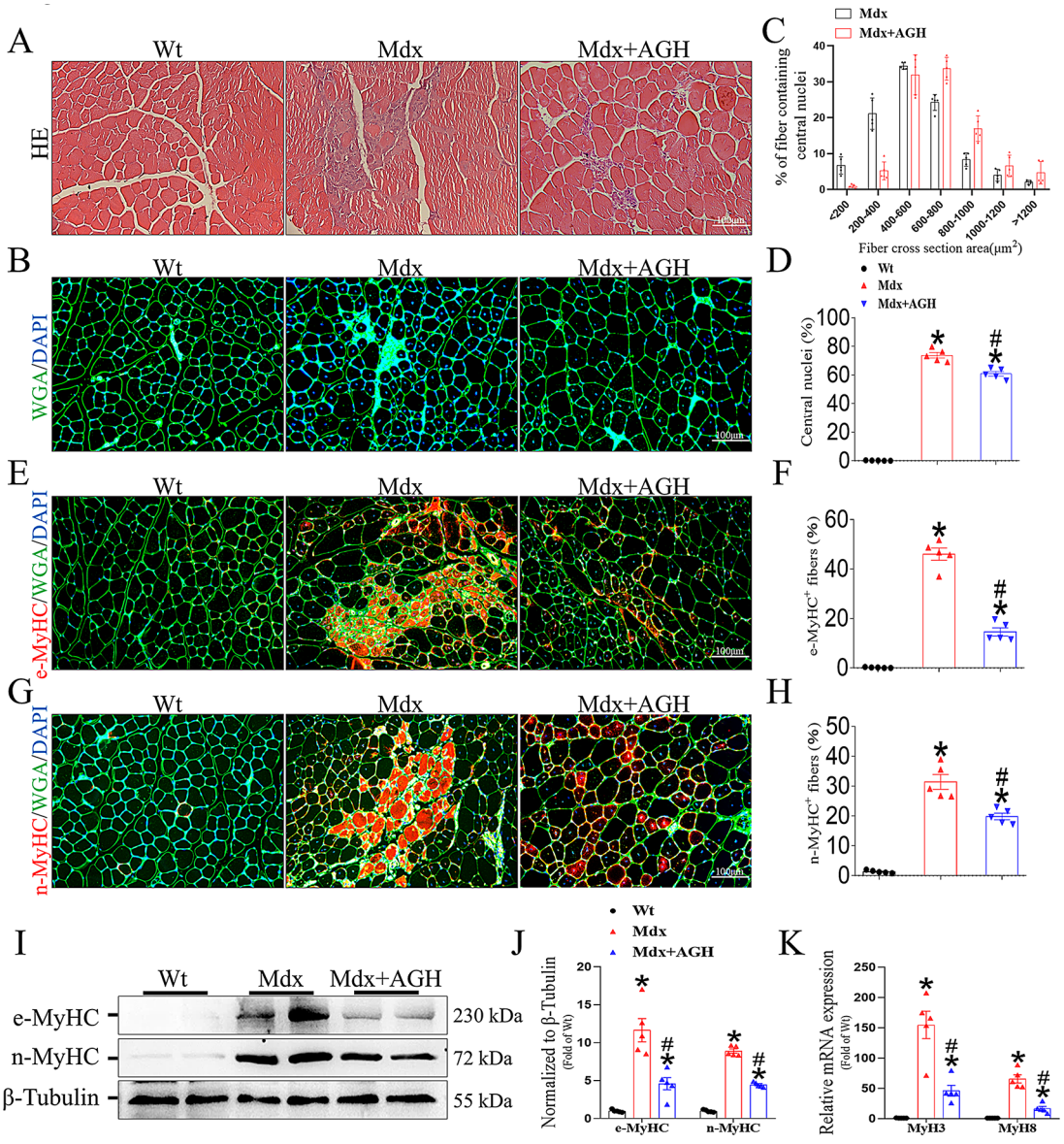


Fig. 5 AGH treatment improved the pathological features of *mdx* muscles while reducing the production of embryonic muscle fiber and neonatal muscle fibers. TA muscles from WT, *mdx*, and AGH-treatment *mdx* mice were isolated at 8 weeks of age. Representative histological images of transverse sections of TA muscle stained with (**A**) Haematoxylin and Eosin and (**B**) wheat germ agglutinin (WGA, green) and DAPI (blue, 20× magnification, scale bar = 100 μm). Proportion of muscle fibers with centrally located (**C**) myonuclei and (**D**) frequency distribution of muscle fiber size. Representative immunofluorescence images and quantification of (**E**–**F**) myosin heavy chain-embryonic (eMyHC, red) and (**G**-**H**) myosin heavy chain-neonatal (nMyHC, red) along with wheat germ agglutinin (WGA, green) and DAPI (blue, 20× magnification, scale bar = 100 μm). (**I**–**J**). Representative blots and quantification for eMyHC and nMyHC normalized to the β-tubulin level. Gene expression levels of (**K**) *MyH3* and *MyH8* were measured using real-time PCR. Values were normalized to 36B4 levels for each target. Values are presented as the mean ± standard error of the mean for each experiment ($n = 5$). * $p < 0.05$ compared with WT control, # $p < 0.05$ compared with *mdx*

myosin, which was increased in *mdx* mice, was significantly reduced following AGH treatment (Fig. 5E–H). These observations were validated at both the protein and gene levels, with AGH treatment significantly reducing embryonic myosin and neonatal myosin expression (Fig. 5I–K).

Taken together, these findings suggest that AGH treatment not only alleviates oxidative stress and mitochondrial autophagy but also enhances muscle regeneration and mitigates morphological abnormalities in the skeletal muscle of *mdx* mice.

AGH restores the fiber type composition in skeletal muscle and improves muscle force

The observed changes in muscle fibers prompted us to investigate whether AGH treatment affects muscle

regeneration and fiber type transition in *mdx* mice. Our findings revealed a significant increase in the expression of *MyH7*, a marker for slow fibers, in *mdx* mice, which slightly decreased following AGH treatment (Fig. 6A). In contrast, *MyH4* expression, indicative of type IIb fast fibers, was reduced in *mdx* mice but was restored to normal levels by AGH treatment (Fig. 6B). The expression of *MyH1* and *MyH2* remained unchanged in *mdx* mice; however, AGH treatment resulted in increased *MyH2* expression (Fig. 6C–D).

Consistent with the *MyH7* gene expression data, immunostaining analysis revealed a notable increase in MyH7-expressing fibers in TA muscles from *mdx* mice. This increase was attenuated by AGH treatment (Fig. 6E, F). The observed changes in fiber type composition likely contributed to the observed changes in body weight and muscle mass in *mdx* mice (Figure S2A–G). Furthermore, compared with *mdx*, AGH treatment significantly improved the muscle force properties of *mdx* mice. Both twitch and tetanic forces, which were markedly lower in *mdx* mice than in WT mice, were significantly greater following AGH treatment, reversing these deficits (Fig. 6G–J). Similarly, grip force and maximum tetanic forces followed the same improvement trend across different electrical frequencies (Fig. 6K–L).

In summary, our results suggest that AGH treatment not only restores the fiber type composition but also significantly improves muscle force impairments in the dystrophic skeletal muscle of *mdx* mice.

AGH alters fiber type composition via the AKT/FOXO1 signaling pathway

Next, we evaluated the expression of the key myogenic transcription factors Pax7, Myf5, MyoD, and myogenin. MyoD is associated primarily with fast fibers, whereas myogenin is characteristic of slow fibers [20, 26]. Consistent with the observed shift in muscle fiber type, we observed increased expression of *Pax7*, *Myf5*, and *MyoD*, accompanied by an approximately 65% reduction in myogenin expression in AGH-treated *mdx* mice compared with *mdx* mice (Fig. 7A–D). Similar to the gene expression results, we observed significantly increased MyoD and reduced myogenin protein levels after AGH treatment (Fig. 7F–H).

In addition, we investigated Foxo1, a critical member of the FOXO family involved in myogenic differentiation and fiber type specification [18, 20]. *Foxo1* gene expression was diminished in *mdx* mice and further reduced following AGH treatment (Fig. 7E). Furthermore, *mdx* mice exhibited increased phosphorylation of Akt and Foxo1 and decreased total protein levels; these effects were enhanced by AGH treatment (Fig. 7F, I–J). In summary, these findings suggest that AGH influences fiber type composition in the TA skeletal muscle of *mdx* mice by modulating the Akt/Foxo1 signaling pathway.

Discussion

Previous studies have reported increased oxidative stress and impaired autophagy in the skeletal muscle of *mdx* mice [27, 28], whereas reactivation of autophagy can improve muscle function and reduce muscle damage [29]. AGH acts as an inhibitor of nitric oxide synthase and ROS. Certain studies have explored the effects of AGH on diabetes complications and cancer [14, 21, 30]; however, our study specifically examines its therapeutic potential in *mdx* mice. Our findings demonstrate that inhibition of autophagy in *mdx* mice leads to the accumulation of damaged mitochondria, as evidenced by impaired mitochondrial integrity and reduced mtDNA levels. Importantly, AGH treatment regulates autophagy and improves muscle force.

Mitochondrial homeostasis relies on a delicate balance between biosynthesis and degradation pathways [31]. Among the pathways involved in mitochondrial degradation, mitophagy mediated by the Pink1/Parkin interaction is particularly noteworthy [32]. Previous studies have consistently shown that damaged mitochondria accumulation in *mdx* mice affects tissues such as the gastrocnemius and diaphragm, and results from disrupted mitophagy characterized by reduced expression of Pink1 and Parkin [33, 34]. These findings are consistent with our results observed in the TA muscles of 8-week-old *mdx* mice. In our study, AGH treatment for two weeks in *mdx* mice resulted in increased mRNA expression levels of *Pink1*, *Parkin*, and *Mfn1*, indicating increased mitophagy and mitochondrial fission, which are critical processes for the clearance of damaged mitochondria. Furthermore, key transcriptional regulators of mitochondrial biogenesis, such as *Pgc1α* and *mtTFA*, were upregulated following AGH treatment [35, 36]. These findings suggest that AGH treatment improved overall mitochondrial integrity by promoting mitochondrial biogenesis.

Oxidative stress arises from increased ROS generation and/or diminished endogenous antioxidant capacity. A limited number of studies have documented elevated oxidative stress in the skeletal muscles of *mdx* mice [6, 37, 38]. Similarly, we observed increased ROS levels in the TA muscle of *mdx* mice, which were reduced by AGH treatment. Moreover, researchers have reported impaired endogenous antioxidant defenses in DMD, including reduced SOD activity and glutathione deficiency, in clinical patients [39–41]. SOD enzymes, particularly MnSOD, are critical for ROS detoxification in mitochondria [42–44]. Additionally, Prdx3, a mitochondria-specific antioxidant enzyme, plays a vital role in maintaining mitochondrial homeostasis and muscle function [45–47]. Consistent with these reports, our results provide evidence of reduced gene and protein expression

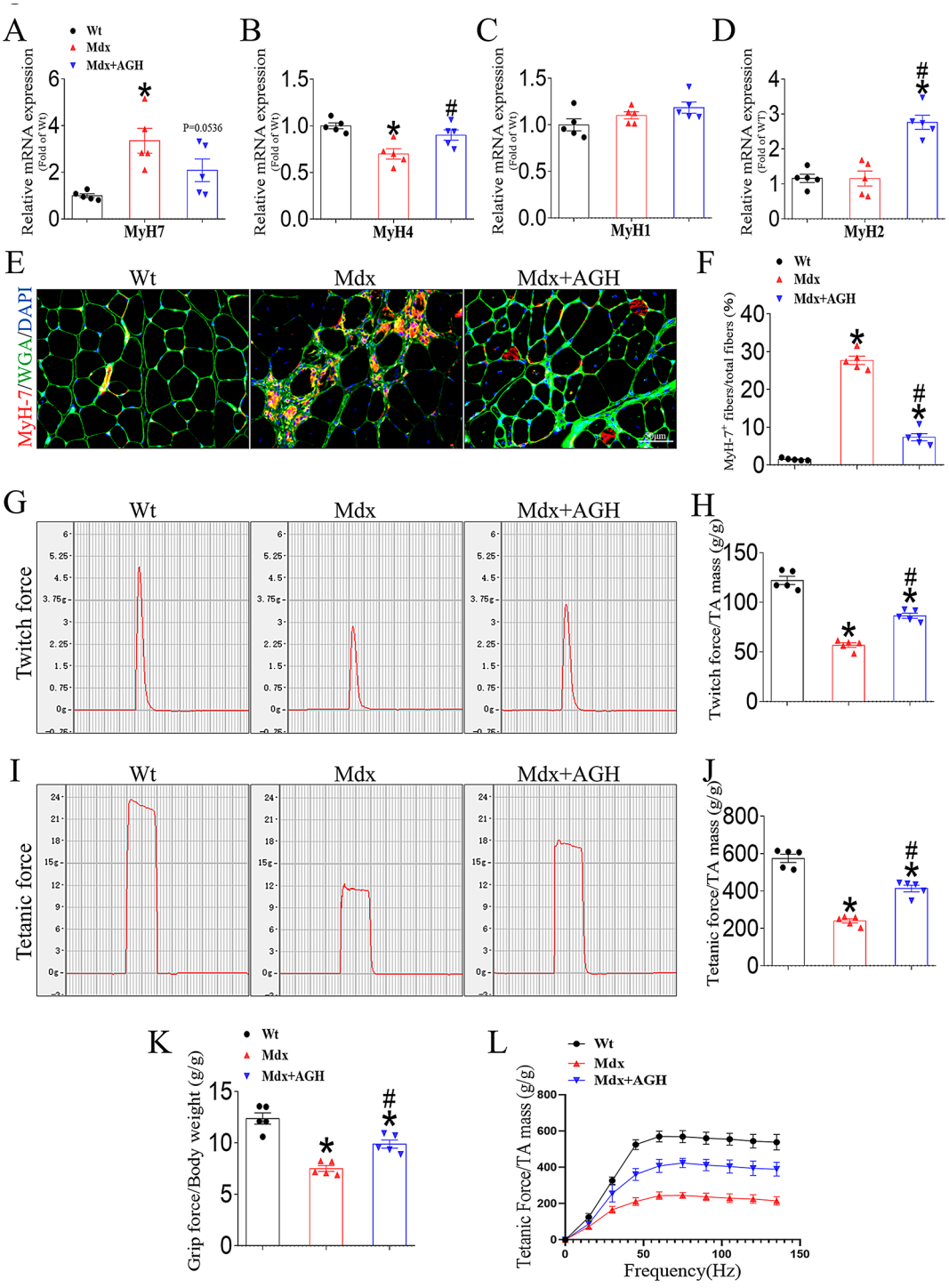


Fig. 6 AGH treatment altered fiber type composition and improved muscle force in *mdx* mice. TA muscles from WT, *mdx*, and AGH-treatment *mdx* mice were isolated at 8 weeks of age. Gene expression of (**A**) *MyH7*, (**B**) *MyH4*, (**C**) *MyH1*, and (**D**) *MyH2* were measured using real-time PCR and values were normalized to 36B4 levels. Representative immunofluorescence images for (**E**) MyH7 (red), wheat germ agglutinin (WGA, green) and DAPI (blue, 20× magnification, scale bar = 50 μm) and (**F**) quantification of the relative ratio of MyH7 positive fibers. Representative images of (**G**–**I**) the twitch force and tetanic force of TA muscle, respectively. Quantification of (**H**) maximum twitch force (**J**) tetanic force and (**L**) changes in the maximum tetanic force at different frequencies normalized to TA muscle mass. Quantification of (**K**) grip force normalized to body weight. Values are presented as the mean ± standard error of the mean for each experiment ($n = 5$). * $p < 0.05$ compared with WT control, # $p < 0.05$ compared with *mdx*

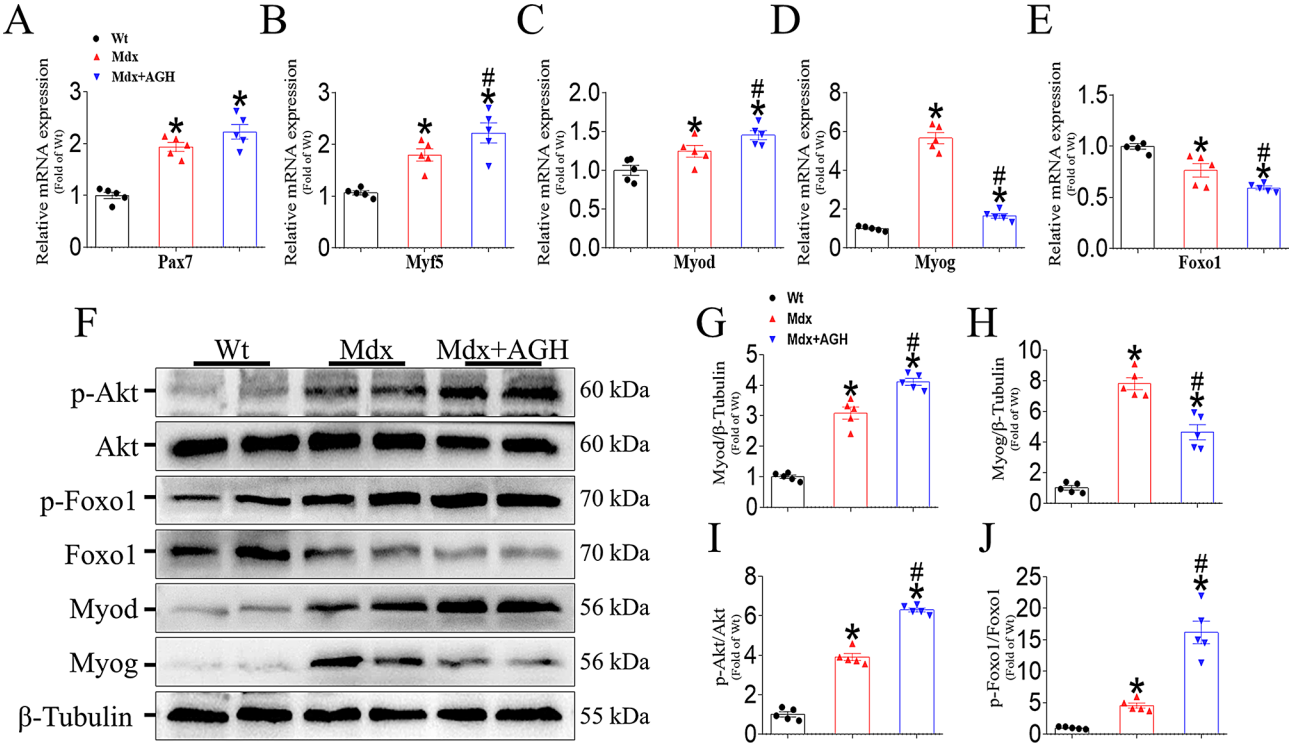


Fig. 7 AGH altered fiber type composition via the AKT/FOXO1 signaling pathway. TA muscles from WT, *mdx*, and AGH-treatment *mdx* mice were isolated at 8 weeks of age. Gene expression of (**A**) *Pax7*, (**B**) *Myf5*, (**C**) *MyoD*, (**D**) *Myog*, and (**E**) *Foxo1* were measured using real-time PCR and values were normalized to 36B4 levels. (**F**–**J**) Representative blots and quantifications for p-Akt, Akt, p-Foxo1, Foxo1, MyoD, and Myog. Values were normalized to β-tubulin. Values are presented as the mean ± standard error of the mean for each experiment ($n = 5$). * $p < 0.05$ compared with WT control, # $p < 0.05$ compared with *mdx*

of MnSOD and Prdx3 in *mdx* mice, which was effectively reversed by AGH treatment.

Glutathione, an essential intracellular antioxidant, exists in both reduced (GSH) and oxidized (GSSG) states [48]. Our study demonstrated for the first time that AGH treatment effectively restored the imbalance in the GSSG/GSH ratio in *mdx* mice, thereby normalizing the GSH system. Furthermore, increased activities of GSH peroxidase and GSH reductase were initially observed in the muscle of *mdx*, indicating early activation of antioxidant defense. However, AGH treatment reduced these activities, probably through restoration of the GSSG/GSH balance and reduced GSSG levels.

Elevated ROS levels can trigger apoptosis, a process observed in the muscle tissue of *mdx* mice [49, 50]. In our study, AGH treatment significantly reduced the number of apoptotic cells in the TA muscle of *mdx* mice. Overall, AGH demonstrated both antioxidant and antiapoptotic properties in the muscle tissue of *mdx* mice.

Structural abnormalities in dystrophic muscle occur because of muscle fiber damage and degeneration [51]. Our study demonstrated that AGH ameliorates these structural changes in TA muscle through its roles in mitophagy, oxidative stress reduction, and apoptosis prevention. Specifically, AGH treatment resulted in a substantial reduction in the number of centralized myonuclei and decreased the number of embryonic and neonatal muscle fibers. Additionally, we observed a rightward shift in the frequency distribution of the cross-sectional areas of the fibers under AGH treatment. These observations suggest that AGH treatment can significantly improve the muscle pathophysiology of *mdx* mice.

Skeletal muscle regeneration in *mdx* mice occurs in a period of hyper-compensation, where satellite cells are activated in response to muscle damage and re-enter the cell cycle. After proliferating, these progenitors exit the cell cycle, differentiate, and either fuse with damaged muscle fibers for repair or with each other to form new fibers [52]. During this process, proliferating myoblasts overexpress Pax7, which inhibits myogenin expression, promoting a quiescent state to preserve the satellite cell pool for future muscle regeneration [53]. Our findings indicate that AGH treatment significantly increased *Pax7*, *Myf5*, and *MyoD* gene expression while decreasing Myog and e-MyHC expression in the TA muscle of *mdx* mice. These results suggest that AGH enhances satellite cell self-renewal and reduces muscle fiber damage, thereby promoting regeneration.

In addition to these cellular effects, AGH treatment also influenced fiber type composition. Previous studies have shown that *mdx* mice exhibit an increased proportion of type I fibers in muscles such as the pectoral, quadriceps, and soleus [54–56], while type IIa fibers are typically decreased, with type IIb and IIx fibers remaining largely unaffected [56, 57]. Our results support these observations, as we found an increased proportion of type I fibers in the TA muscle of *mdx* mice following AGH treatment, alongside a decrease

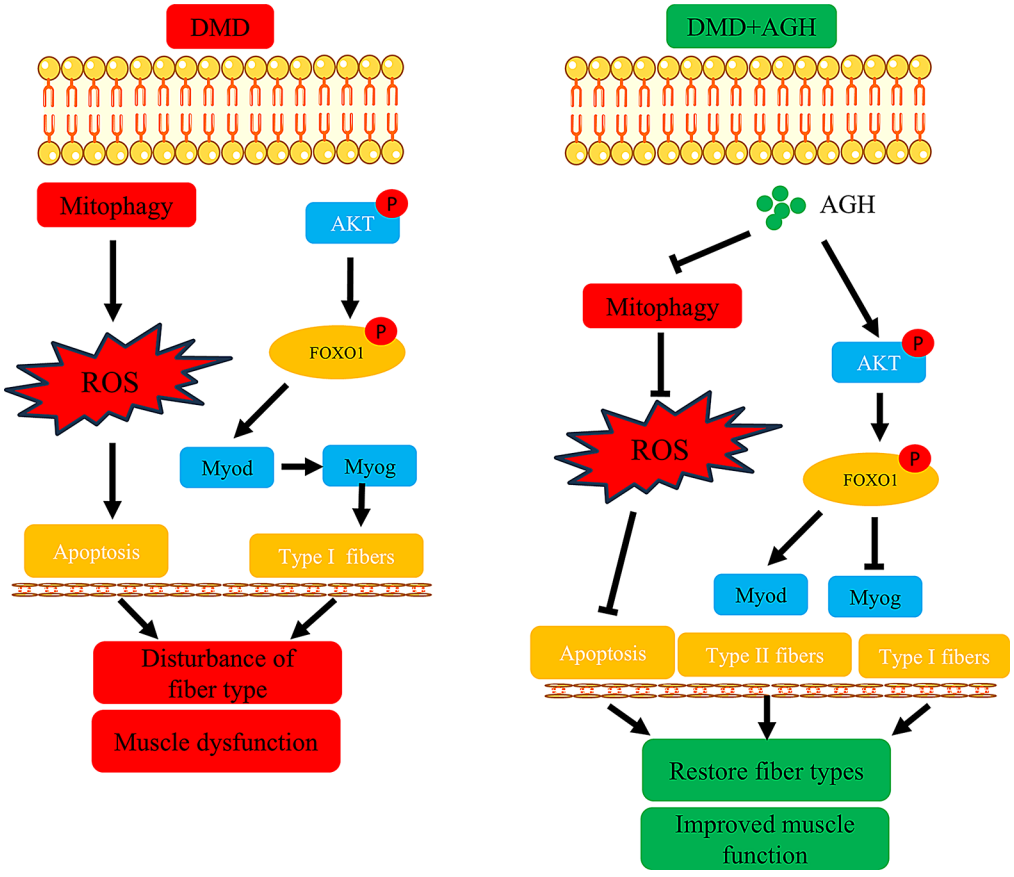


Fig. 8 Summary diagram of AGH treatment in *mdx* mice. AGH treatment reduced ROS and apoptosis by restoring mitochondrial autophagy, restored the composition of muscle fiber types, and improved muscle force through the AKT/FOXO1 signaling pathway

in the gene expression of *MyH4* and no significant change in *MyH1* or *MyH2* expression. Interestingly, AGH treatment also decreased the proportion of type I slow fibers and increased the expression of type IIa and type IIb fast fibers, suggesting a shift in fiber type composition toward faster-twitch fibers.

The changes in fiber type composition observed with AGH treatment may be linked to improved muscle force-generating capacity. High ROS levels are known to impair muscle force production [58], and the altered redox balance in *mdx* mice contributes to muscle weakness [59, 60]. Muscle fiber type is a key determinant of contractility and metabolism, and AGH treatment's effects on fiber type composition were associated with significant improvements in grip strength, as well as twitch and tetanic force in the TA muscle of *mdx* mice. These findings highlight the novel role of AGH in improving both muscle fiber composition and force generation, potentially through its effects on mitochondrial dynamics and oxidative stress regulation.

At the molecular level, AKT signaling plays a pivotal role in muscle hypertrophy, myofiber growth, and the prevention of atrophy [61–63]. In particular, activation of the AKT signaling pathway has been shown to mitigate muscle degeneration and enhance muscle regeneration in dystrophin-deficient *mdx* mice [64]. Our results are consistent with these studies, as we observed activation of AKT signaling in the skeletal muscle of *mdx* mice, which was further enhanced by AGH treatment.

Foxo1, a transcription factor involved in growth suppression, apoptosis, and muscle atrophy, is regulated by AKT signaling through phosphorylation at key sites like Thr24 and Ser316 [65]. In *mdx* mice, Foxo1 phosphorylation levels are elevated, but its nuclear localization is reduced, suggesting dysregulated activity [27]. Foxo1 is also crucial in regulating muscle fiber type specification. Conditional ablation of Foxo1 in skeletal muscle promotes the formation of type II fibers and alters the balance of fiber types, favoring type II fibers at the expense of type I fibers. The upregulation and activation of Foxo1, together with Foxo3a and Myog, likely contribute to the expression of catabolic genes such as MAFbx and MuRF1, which are involved in muscle remodeling and atrophy [19]. Our data suggest that AGH treatment modulates AKT/FOXO1 signaling, leading to altered fiber type composition and improved muscle function. Therefore, AGH treatment not only affects fiber type composition but also has the potential to attenuate pathological muscle events in *mdx* mice.

Conclusions

This study reveals that AGH has significant therapeutic potential in the *mdx* mouse model of DMD by effectively restoring mitochondrial integrity, reducing oxidative stress, and modulating the *AKT*/*FOXO1* signaling pathway (Fig. 8). These molecular actions lead to improved

muscle fiber composition and enhanced muscle force, as evidenced by increased grip strength and twitch force. By addressing the key pathological features of DMD, AGH offers a promising new avenue for treatment, with the potential to significantly slow disease progression. These findings lay the groundwork for future research aimed at optimizing AGH as a targeted therapy for muscular dystrophies, bringing us closer to viable clinical interventions.

Abbreviations

AGH	Aminoguanidine hemisulfate
DMD	Duchenne muscular dystrophy
ROS	Reactive oxygen species
Pgc1α	Peroxisome proliferator-activated receptor gamma coactivator-1 alpha
TA	Tibialis anterior
WT	Wild-type
MnSOD	Manganese superoxide dismutase
GSH	Glutathione
GSSG	Oxidized glutathione
DHE	Dihydroethidium

Supplementary Information

The online version contains supplementary material available at https://doi.org/10.1186/s13395-024-00371-1.

Supplementary Material 1

Acknowledgements
We would like to thank Editage (https://www.editage.cn) for English language editing.

Author contributions
S. S. and H. M. A. J. conceived and designed the research; S. S., T. Y., and Y. C. performed experiments; S. S., T. Y., J. Y. H, and H. M. A. J. analyzed and interpreted the results of the experiments; S. S., and S. Y. prepared figures; S. S., T. Y., and S. Y. drafted the manuscript. S. Y., and H. M. A. J. edited and revised the manuscript; H. M. A. J provided the funding. All authors approved the final version of the manuscript.

Funding
This study was supported by the Second Affiliated Hospital of Wenzhou Medical University Fund (No. KT20240305161402346).

Data availability
The authors confirm that data supporting the findings of this study are available within the article and supplementary material.

Declarations

Ethics approval and consent to participate
The animal study protocol was approved by the Institutional Animal Ethics Committee of the Laboratory Animal Resources Center (protocol code: wydw2022-0606; Date: September 2022).

Consent for publication
Not applicable.

Competing interests
The authors declare no competing interests.

Author details
[1]College of Pharmacy, Chonnam National University, Gwangju, Republic of Korea
[2]Department of Anesthesia and Critical Care, The Second Affiliated Hospital of Wenzhou Medical University, Wenzhou, China
[3]College of Pharmacy, Wenzhou Medical University, Wenzhou, China
[4]College of Pharmacy, Chung-Ang University, Seoul, Republic of Korea
[5]Department of Global Innovative Drugs, The Graduate School of Chung-Ang University, Seoul, Republic of Korea

Received: 24 September 2024 / Accepted: 23 December 2024
Published online: 13 January 2025

References

1. Fawzy AS, Gabriele S, Corrado A. Advances in Dystrophinopathy diagnosis and therapy. Biomolecules. 2023;13(9).
2. Duan D, Goemans N, Takeda S, Mercuri E, Aartsma-Rus A. Duchenne muscular dystrophy. Nat Reviews Disease Primers. 2021;7(1):13.
3. Hoffman E, Brown R, Kunkel L. Dystrophin: the protein product of the Duchenne muscular dystrophy locus. Cell. 1987;51(6):919–28.
4. Pal R, Palmieri M, Loehr J, Li S, Abo-Zahrah R, Monroe T, et al. Src-dependent impairment of autophagy by oxidative stress in a mouse model of Duchenne muscular dystrophy. Nat Commun. 2014;5:4425.
5. Olga M, Katarzyna K, Paulina P, Kinga R, Józef D, Agnieszka Ł. Dysregulated autophagy and Mitophagy in a mouse model of Duchenne muscular dystrophy remain unchanged following heme Oxygenase-1 knockout. Int J Mol Sci. 2022;23(1).
6. Rio S, Atsushi K, Ryusuke H, Takashi H, Yoshiyuki H. Resveratrol decreases oxidative stress by restoring Mitophagy and improves the pathophysiology of Dystrophin-Deficient mdx mice. Oxid Med Cell Longev. 2018;2018:0.
7. Lorenzo G, Oliver K, Christina T-H, Guido K. Mitochondrial control of cellular life, stress, and death. Circ Res. 2012;111(9).
8. Ruohai L, Pengpeng J, Liqun Y, Ying W, Liping H, Tong S et al. Impaired mitochondrial dynamics and bioenergetics in diabetic skeletal muscle. PLoS ONE. 2014;9(3).
9. LeBleu V, O'Connell J, Gonzalez Herrera K, Wikman H, Pantel K, Haigis M, et al. PGC-1α mediates mitochondrial biogenesis and oxidative phosphorylation in cancer cells to promote metastasis. Nat Cell Biol. 2014;16(10):992–1003.
10. Ashrafi G, Schwarz T. The pathways of mitophagy for quality control and clearance of mitochondria. Cell Death Differ. 2013;20(1):31–42.
11. McWilliams T, Muqit M. PINK1 and Parkin: emerging themes in mitochondrial homeostasis. Curr Opin Cell Biol. 2017;45:83–91.
12. Magdalena K, Katarzyna P-G, Alicja J, Jozef D. The role of oxidative stress in skeletal muscle injury and regeneration: focus on antioxidant enzymes. J Muscle Res Cell Motil. 2016;36(6).
13. David PB, Sarah ED, Dearbhla B, Amélie C, Kevin HM, Deirdre E et al. N-acetylcysteine decreases fibrosis and increases Force-Generating Capacity of Mdx Diaphragm. Antioxid (Basel). 2019;8(12).
14. Po-Li W, Chin-Sheng H, Hsuan-Hsuan L, Uyanga B, Chien-Yu H, Yu-Jia C. Areca nut extract (ANE) inhibits the progression of hepatocellular carcinoma cells via activation of ROS production and activation of autophagy. Int J Med Sci. 2021;18(15).
15. Vazquez-Torres A, Jones-Carson J, Mastroeni P, Ischiropoulos H, Fang F. Antimicrobial actions of the NADPH phagocyte oxidase and inducible nitric oxide synthase in experimental salmonellosis. I. effects on microbial killing by activated peritoneal macrophages in vitro. J Exp Med. 2000;192(2):227–36.
16. Accili D, Arden K. FoxOs at the crossroads of cellular metabolism, differentiation, and transformation. Cell. 2004;117(4):421–6.
17. Furuyama T, Nakazawa T, Nakano I, Mori N. Identification of the differential distribution patterns of mRNAs and consensus binding sequences for mouse DAF-16 homologues. Biochem J. 2000;349:629–34.
18. Xu M, Chen X, Chen D, Yu B, Huang Z. FoxO1: a novel insight into its molecular mechanisms in the regulation of skeletal muscle differentiation and fiber type specification. Oncotarget. 2017;8(6):10662–74.
19. Zhang Y, Aguilar O, Storey K. Transcriptional activation of muscle atrophy promotes cardiac muscle remodeling during mammalian hibernation. PeerJ. 2016;4:e2317.
20. Kitamura T, Kitamura Y, Funahashi Y, Shawber C, Castrillon D, Kollipara R, et al. A Foxo/Notch pathway controls myogenic differentiation and fiber type specification. J Clin Investig. 2007;117(9):2477–85.
21. Fábio Cangeri DN, Graziella R, Alexandre SD, Marilene P, Henrique F, Norma Possa M. Hepatic nitrosative stress in experimental diabetes. J Diabetes Complications. 2012;26(5).

22. Kun H, Dan-Dan W, Wen-Bao H, Wei-Qian Z, Xia X, Qiu-Xiang L et al. Calcitriol increases MBNL1 expression and alleviates myotonic dystrophy phenotypes in HSA(LR) mouse models. J Transl Med. 2022;20(1).
23. Gregory O, Alissa R, Prameela B, Leatha C, Cory WB, Brian CC et al. Optimization and construct validity of approaches to preclinical grip strength testing. J Cachexia Sarcopenia Muscle. 2023;14(5).
24. Xin-Huang L, Xiao-Xia C, Jin-Liang N, Xing-Mei L, Qian-Li Z, Jian S et al. Anti-diabetic drug canagliflozin hinders skeletal muscle regeneration in mice. Acta Pharmacol Sin. 2022;43(10).
25. Skulachev V. Mitochondria-targeted antioxidants as promising drugs for treatment of age-related brain diseases. J Alzheimer's Disease: JAD. 2012;28(2):283–9.
26. S M H, J M T, S J T, C M G, W J C. C a P. Selective accumulation of MyoD and myogenin mRNAs in fast and slow adult skeletal muscle is controlled by innervation and hormones. Development. 1993;118(4).
27. Nakashima R, Hosoda R, Tatekoshi Y, Iwahara N, Saga Y, Kuno A. Transcriptional dysregulation of autophagy in the muscle of a mouse model of Duchenne muscular dystrophy. Sci Rep. 2024;14(1):1365.
28. Spitali P, Grumati P, Hiller M, Chrisam M, Aartsma-Rus A, Bonaldo P. Autophagy is impaired in the Tibialis Anterior of Dystrophin null mice. PLoS Curr. 2013;5.
29. De Palma C, Morisi F, Cheli S, Pambianco S, Cappello V, Vezzoli M, et al. Autophagy as a new therapeutic target in Duchenne muscular dystrophy. Cell Death Dis. 2012;3(11):e418.
30. You-Ting Z, Lin-Li L, Tian-Tian L, Xiao L, Jin-Long Y. Effects of L-arginine on nitric oxide synthesis and larval metamorphosis of Mytilus coruscus. Genes (Basel). 2023;14(2).
31. Shifu A, Vijay S, Arijit C, Sujin C, Alexandra D, Claire, dC et al. Skeletal muscle mitochondrial dysfunction mediated by Pseudomonas aeruginosa quorum-sensing transcription factor MvfR: reversing effects with anti-MvfR and mitochondrial-targeted compounds. mBio. 2024.
32. Jin S, Youle R. PINK1- and parkin-mediated mitophagy at a glance. J Cell Sci. 2012;125:795–9.
33. Mucha O, Kaziród K, Podkalicka P, Rusin K, Dulak J, Łoboda A. Dysregulated autophagy and Mitophagy in a mouse model of Duchenne muscular dystrophy remain unchanged following heme Oxygenase-1 knockout. Int J Mol Sci. 2021;23(1).
34. Kang C, Badr M, Kyrychenko V, Eskelinen E, Shirokova N. Deficit in PINK1/PARKIN-mediated mitochondrial autophagy at late stages of dystrophic cardiomyopathy. Cardiovascular Res. 2018;114(1):90–102.
35. G D W GKM. Effect of nitric oxide synthase inhibition on mitochondrial biogenesis in rat skeletal muscle. J Appl Physiol (1985). 2006;102(1).
36. Hafiz Muhammad Ahmad J, Hwayeon L, Sooim S, Joo Young H. Inhibition of autophagy with chloroquine dysregulates mitochondrial quality control and energetics in adipocytes. Arch Pharm Res. 2022;45(10).
37. Kevin ES, Alex RA, Jeovanna L, Muthu P, Frederick AV, Jlll A R-F et al. Muscle damage, metabolism, and oxidative stress in mdx mice: impact of aerobic running. Muscle Nerve. 2015;54(1).
38. Sılasu A, Nuray A, Dilek Ö, Merve Açıkel E, Serap A, Guldal S. Effects of moderate aerobic exercise, low-level laser therapy, or their combination on muscles pathology, oxidative stress and irisin levels in the mdx mouse model of Duchenne muscular dystrophy. Lasers Med Sci. 2022;37(7).
39. Burr IM, Asayama K, Fenichel GM. Superoxide dismutases, glutathione peroxidase, and catalase in neuromuscular disease. Muscle & Nerve: Official Journal of the American Association of Electrodiagnostic Medicine. 1987;10(2):150–4.
40. Lara K, Marie-Claude B, Christo C, Thibaud D, Brigitte E, Philippe C et al. Delayed cardiomyopathy in dystrophin deficient mdx mice relies on intrinsic glutathione resource. Am J Pathol. 2010;177(3).
41. Renjini R, Gayathri N, Nalini A, Srinivas Bharath MM. Oxidative damage in muscular dystrophy correlates with the severity of the pathology: role of glutathione metabolism. Neurochem Res. 2012;37(4).
42. Weydert C, Cullen J. Measurement of superoxide dismutase, catalase and glutathione peroxidase in cultured cells and tissue. Nat Protoc. 2010;5(1):51–66.
43. Van Remmen H, Ikeno Y, Hamilton M, Pahlavani M, Wolf N, Thorpe S, et al. Life-long reduction in MnSOD activity results in increased DNA damage and higher incidence of cancer but does not accelerate aging. Physiol Genom. 2003;16(1):29–37.
44. Candas D, Li J. MnSOD in oxidative stress response-potential regulation via mitochondrial protein influx. Antioxid Redox Signal. 2014;20(10):1599–617.
45. Chen L, Na R, Gu M, Salmon A, Liu Y, Liang H, et al. Reduction of mitochondrial H2O2 by overexpressing peroxiredoxin 3 improves glucose tolerance in mice. Aging Cell. 2008;7(6):866–78.
46. Lee K, Shin Y, Cho S, Lee S, Bahn Y, Kim J, et al. Peroxiredoxin 3 has a crucial role in the contractile function of skeletal muscle by regulating mitochondrial homeostasis. Free Radic Biol Med. 2014;77:298–306.
47. Zhang Y, Wang L, Kaifu T, Li J, Li X, Li L. Featured article: accelerated decline of physical strength in peroxiredoxin-3 knockout mice. (Maywood NJ). 2016;241(13):1395–400. Experimental biology and medicine.
48. Kwon D, Cha H, Lee H, Hong S, Park C, Park S et al. Protective effect of glutathione against oxidative stress-induced cytotoxicity in RAW 264.7 macrophages through activating the Nuclear factor erythroid 2-Related Factor-2/Heme Oxygenase-1 pathway. Antioxidants (Basel, Switzerland). 2019;8(4).
49. Martin O, Vladimir G, Sten O, Boris Z. Mitochondria, oxidative stress and cell death. Apoptosis. 2007;12(5).
50. Hermes T, Mâncio R, Mizobutti D, Macedo A, Kido L, Cagnon Quitete V, et al. Cilostazol attenuates oxidative stress and apoptosis in the quadriceps muscle of the dystrophic mouse experimental model. Int J Exp Pathol. 2023;104(1):13–22.
51. Burns D, Drummond S, Bolger D, Coiscaud A, Murphy K, Edge D et al. Mdxn-acetylcysteine decreases fibrosis and increases Force-Generating Capacity of Diaphragm. Antioxid (Basel Switzerland). 2019;8(12).
52. Hugo CO, Addolorata P. Marking the tempo for myogenesis: Pax7 and the regulation of muscle stem cell fate decisions. J Cell Mol Med. 2011;16(5).
53. Valentina F, Rachel SG, Philipp A, Amy R, Jeremy ET, Addolorata P. The Satellite Cell Niche regulates the balance between myoblast differentiation and Self-Renewal via p53. Stem Cell Rep. 2018;10(3).
54. Voit A, Patel V, Pachon R, Shah V, Bakhutma M, Kohlbrenner E, et al. Reducing sarcolipin expression mitigates Duchenne muscular dystrophy and associated cardiomyopathy in mice. Nat Commun. 2017;8(1):1068.
55. Schneider J, Shanmugam M, Gonzalez J, Lopez H, Gordan R, Fraidenraich D, et al. Increased sarcolipin expression and decreased sarco(endo)plasmic reticulum Ca2 + uptake in skeletal muscles of mouse models of Duchenne muscular dystrophy. J Muscle Res Cell Motil. 2013;34:349–56.
56. Spassov A, Gredes T, Gedrange T, Lucke S, Morgenstern S, Pavlovic D, et al. Differential expression of myosin heavy chain isoforms in the masticatory muscles of dystrophin-deficient mice. Eur J Orthod. 2011;33(6):613–9.
57. Péladeau C, Adam N, Jasmin B. Celecoxib treatment improves muscle function in mdx mice and increases utrophin A expression. FASEB Journal: Official Publication Federation Am Soc Experimental Biology. 2018;32(9):5090–103.
58. M B R. Invited Review: redox modulation of skeletal muscle contraction: what we know and what we don't. J Appl Physiol (1985). 2001;90(2).
59. Lawler J. Exacerbation of pathology by oxidative stress in respiratory and locomotor muscles with Duchenne muscular dystrophy. J Physiol. 2011;589:2161–70.
60. Kim J, Kwak H, Thompson L, Lawler J. Contribution of oxidative stress to pathology in diaphragm and limb muscles with Duchenne muscular dystrophy. J Muscle Res Cell Motil. 2013;34(1):1–13.
61. Rommel C, Bodine S, Clarke B, Rossman R, Nunez L, Stitt T, et al. Mediation of IGF-1-induced skeletal myotube hypertrophy by PI(3)K/Akt/mTOR and PI(3)K/Akt/GSK3 pathways. Nat Cell Biol. 2001;3(11):1009–13.
62. Akihiro T, Yasuko K, Jiang Y, Zhengyu L, Kun G, Debabrata M et al. Myogenic akt signaling regulates blood vessel recruitment during myofiber growth. Mol Cell Biol. 2002;22(13).
63. Bodine SC, Stitt TN, Gonzalez M, Kline WO, Stover GL, Bauerlein R, et al. Akt/mTOR pathway is a crucial regulator of skeletal muscle hypertrophy and can prevent muscle atrophy in vivo. Nature cell biology. 2001;3(11):1014–9.
64. Michelle HK, Danielle IK, Renuka TR, Bo Ming C, Nigel H, Yasuhiro I et al. Myogenic akt signaling attenuates muscular degeneration, promotes myofiber regeneration and improves muscle function in dystrophin-deficient mdx mice. Hum Mol Genet. 2011;20(7).
65. Nakae J, Barr V, Accili D. Differential regulation of gene expression by insulin and IGF-1 receptors correlates with phosphorylation of a single amino acid residue in the forkhead transcription factor FKHR. EMBO J. 2000;19(5):989–96.

Publisher's note

Springer Nature remains neutral with regard to jurisdictional claims in published maps and institutional affiliations.